Electronic structure of indium-tin-oxide films fabricated by reactive electron-beam deposition

F. Matino,* L. Persano, V. Arima, D. Pisignano, R. I. R. Blyth, R. Cingolani, and Ross Rinaldi
National Nanotechnology Laboratory of INFM-CNR, Distretto Tecnologico ISUFI, Universita' di Lecce, Via Arnesano, 73100 Lecce, Italy
(Received 24 March 2005; published 16 August 2005)

Thin films of indium tin oxide [(ITO), In_2O_3:Sn] have been grown by reactive electron beam deposition. Annealing in ultrahigh vacuum and, subsequently, *in situ* room temperature scanning tunneling microscopy (STM) and spectroscopy have been carried out. STM images before annealing show the film composed of grains with sizes around 30 nm while images of samples annealed at 423 K and 573 K indicate that these grains coalesce with sizes of 60–80 nm. Scanning tunneling spectroscopy (STS) curves for the samples in the three different conditions indicate the existence of a small band gap with Fermi level position pinned in the center of the band gap. Optical reflectance and transmittance measurements have been performed in order to deduce optical and electronic properties. STS combined with optical data interpreted with Drude theory shows that the samples have a direct band gap of 3.5 (±0.1) eV and an indirect band gap of 2.1 (±0.2) eV.

DOI: 10.1103/PhysRevB.72.085437 PACS number(s): 73.20.At, 68.37.Ef, 78.40.Ha

I. INTRODUCTION

In recent years, materials exhibiting high transparency at visible wavelengths and good electrical conductance, particularly transparent conducting oxides, have been the subject of several studies, in view of their use as substrates for widespread applications, including liquid crystal and field emission displays, plasma panels, solar cells, organic electroluminescent, and electrochromic devices.[1–4]

These applications require a combination of high transparency in the visible region (~90%), with resistivity as low as $\approx 10^{-4}$ Ω cm, which involves the design and the creation of electron degeneracy in wide-gap oxides (≥3 eV) by introducing appropriate dopants. Such requirements can be satisfied by a large number of conductive oxides of cadmium, tin, zinc, indium, and their alloys in film form.[5] In particular, indium tin oxide [(ITO), In_2O_3:Sn] is one of the most widely used and extensively studied, conductive oxides.[4]

ITO is a heavily doped, *n*-type semiconductor, with an optical band gap of 3–4 eV, whose high transparency and conductivity strongly depend on the different manufacturing techniques, and particularly on the substrate temperature during growth[6] and on postdeposition treatments, such as thermal annealing or plasma processes.[7,8]

Because of the broad interest in the technological applications of ITO, a deeper knowledge of the correlation between its structural and electronic properties, as well as the understanding of its surface and interface physics, is required in order to obtain enhanced performances in optoelectronic devices. It is well known, indeed, that not only morphological variations on the nanoscale range can have a significant impact on device characteristics, but also changes in the interface properties can lend to irreproducible metal-semiconductor contacts and/or Schottky barriers limiting the performances of devices. For these reasons, the surface electronic structure of ITO needs to be investigated in depth.

Several different techniques have been used to investigate the properties of ITO, such as ellipsometry,[9] x-ray photoelectron spectroscopy,[10] photoemission spectroscopy,[11,12] x-ray diffraction,[13] variable angle reflectance FTIR (Fourier transform infrared spectroscopy),[14] optical transmission, and reflectance measurements,[4] but although it has been widely studied, its electronic structure is not completely known.

In particular, Hamberg *et al.*[15] analyzed the optical and transport properties, using a one-dimensional model to deduce the electronic band structure, whereas Mryasov *et al.*[16] reported first-principles [full potential linear muffin-tin orbital (FLMTO)] calculations of the electronic band structure for In_2O_3 and Sn-doped In_2O_3, and Errico *et al.*[17]considered pure and Cd-doped In_2O_3 using full potential and lattice relaxations. The main obstacles to theoretical work are the large unit cell of crystalline In_2O_3, which consists of 80 atoms,[18] and the complex nature of the conductive mechanism in Sn-doped In_2O_3.[3,13,18]

Scanning tunneling microscopy (STM) and scanning tunneling spectroscopy (STS) can be powerful tools to obtain information about surface local electronic structure. Being sensitive to the electronic states within the energy window determined by the applied bias voltage, STM is able to obtain both atomic scale resolved topographical images of the sample surface, and to measure (by positioning the tip over a selected surface site) the current-voltage (I-V) characteristics, thus providing information about the site-specific local density of states (LDOS).

In addition, the preparation of ITO films to achieve the required optical or electronic properties is still a matter of study. So far, many different deposition techniques have been reported in the literature, such as dc (Ref. 13) and rf (Ref. 19) magnetron sputtering, spray pyrolysis,[20] thermal evaporation,[21] chemical vapor,[22] and electron-beam deposition.[10] In particular, commercially available conducting transparent oxides for electroactive devices are usually deposited by sputtering techniques which, however, produce films of relatively high roughness on the nanometer scale (for commercially available ITO typical rms roughness values are in the range 10–20 nm), which in turn poses many problems for an effective deposition of the active layers.[23] Electron-beam evaporation permits to overcome these problems, enabling the fabrication of layers of conducting oxide with very low roughness values.

In this paper we report a STM analysis of surface morphological and electronic structure of ITO films fabricated by reactive electron-beam deposition, to which were also applied annealing treatments in order to investigate possible changes in ITO structure. With the aim of confirming band gap information and electronic properties provided by STS data, we also carried out characterization by optical reflectance and transmission measurements in the visible to near-IR range, interpreting the results using a Drude free-electron model.

II. EXPERIMENT

Thin films of ITO were deposited on Corning glass and *n*-doped silicon substrates by reactive electron-beam evaporation. The evaporation chamber was evacuated to a base pressure of 4×10^{-6} mbar. A controlled oxygen atmosphere was achieved via a gas inlet through a precision needle valve. The films were deposited from 99.9% purity $In_2O_3:Sn$ (90 and 10 wt %, respectively) pieces [IAM (International Advanced Materials), NY] at a working pressure of 1.5×10^{-4} mbar. During film growth, the chamber temperature was kept at 530 K by a halogen lamp. The electron-beam source operated at 9 KV, with a constant deposition rate of about 1.0 Å s^{-1}, monitored by a quartz crystal microbalance. ITO samples were introduced, via a load lock, in a UHV chamber (10^{-10} mbar) equipped with an Omicron Variable Temperature (VT) STM, a sample heating facility and a low-energy electron diffraction (LEED)/Auger system. The first sample was measured as- deposited without any modification. The other two were annealed, respectively, at nominal temperatures of 423 K and 573 K; the thermocouple being located close to, but not in direct contact with, the sample by passing a current directly through the sample.

The STM and STS measurements were carried out in UHV at room temperature, using Pt-Ir tips. During spectroscopy measurements, the feedback loop was switched off and the set-point current, which sets the tip-sample distance, was fixed during the bias voltage (V_{bias}) scan. The spectroscopy measurements were performed by collecting grids of points spaced at 2.5 nm after moving the tip to the chosen sites. Different bias voltages and current set points were used to carry out spectroscopic measurements on the three different samples. The STS spectra shown in this paper are averaged over a set of several *I-V* curves in a grid over the scanning area.

Optical measurements were carried out using a Varian Cary 5 Ultra Violet-Visible-Near-Infra Red (UV-VIS-NIR) spectrophotometer in the range from 200 to 3100 nm. Specular reflectance data was acquired using the VW geometry.[24]

III. RESULTS AND DISCUSSION

Auger measurements on the as-deposited sample were carried out in order to determine the In:Sn ratio. Using the In and Sn *MNN* Auger peaks we found an In:Sn ratio of 4:1, rather than the 4.5:1 of the starting material. This suggests that there is preferential evaporation of the (lighter) Sn.

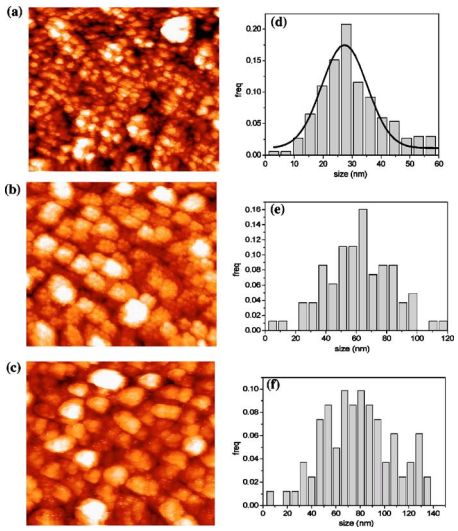

FIG. 1. (Color online) STM images of the ITO films: (a) as-deposited film; (b) annealed at 423 K; (c) annealed at 573 K. $V_{tip}=1$ V, $I_{set\ point}=50$ pA, scan area 1000 nm$\times$1000 nm. (d), (e), and (f) show grain size distributions for samples *a*, *b*, and *c*, respectively.

Figures 1(a)–1(c) show STM images of ITO deposited on silicon on the as-deposited film and after annealing at 423 K and 573 K. Figures 1(d)–1(f) show the grain size distribution for each sample: for as-deposited film [Fig. 1(d)], this distribution is narrow and Gaussian-like, with an average grain size of about 28 nm; whereas for annealed samples the distribution cannot be fit using a simple Gaussian distribution; and the larger size spread is accompanied by somewhat higher values, about 60–80 nm [Figs. 1(e) and 1(f)], for the average grain size. Furthermore, from Fig. 1, (rms) values of 5.7 nm, 6.1 nm, and 7.3 nm, respectively, were determined for the surface roughness of the as-deposited 423 K and 573 K annealed samples. This is due to the aggregation of the native grains into larger clusters upon annealing.

We measured the STS current-voltage characteristics simultaneously with STM images positioning the tip on and between the grains in order to investigate possible differences in electronic properties through dark and bright areas in the STM images. The *I-V* curves in Fig. 2 were obtained as an average of several curves acquired in the dark and bright areas in Fig. 1(a). The two curves show the zero-

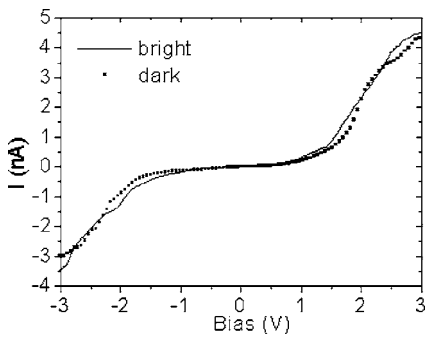

FIG. 2. *I-V* curves on the dark and the bright areas of Fig. 1(a) acquired at $V_{tip}=1$ V and $I_{set\ point}=50$ pA.

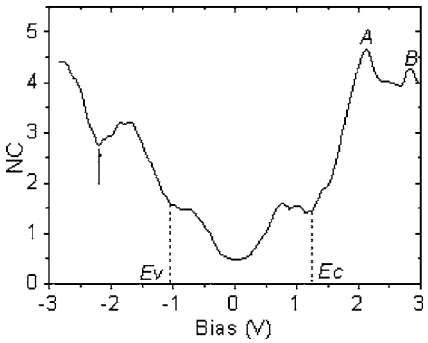

FIG. 3. STS of the as-deposited ITO film. NC was numerically calculated from STS *I-V* curves performed with set point of V_{tip} =3 V and $I_{set\ point}$=50 pA.

current gap typical of semiconductor behavior. However, we did not find significant variations in the *I-V* curves recorded in different areas, unlike Kasiviswanathan *et al.*,[25] who reported different spectroscopic behaviors at the grain boundary, attributed to the presence of excess impurities creating defects at interface region. Our finding indicates instead that the contrasts in the STM image are due to morphological differences in the ITO surface rather than in their electronic structure.

Figures 3 and 4 show the normalized conductance (NC) curves, $(dI/dV)/(I/V)$ vs bias voltage, numerically calculated from *I-V* curves. The NC curves, which are known to be proportional to the surface local density of states (LDOS), were calculated using the method described by Feenstra.[26] The energy positions of the valence and conduction band

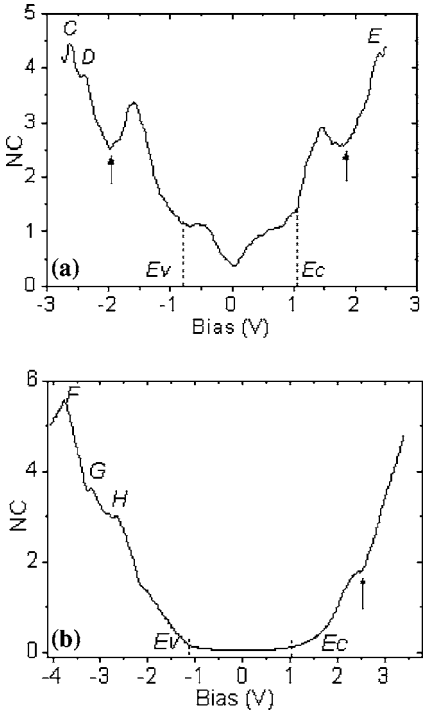

FIG. 4. STS of the ITO film annealed at (a) 423 K and (b) 573 K. NC was numerically calculated from STS *I-V* curves performed with a set point of (a) V_{tip}=2 V and $I_{set\ point}$=50 pA and (b) V_{tip}=3 V and $I_{set\ point}$=300 pA.

onsets can be established in NC spectra using the procedure shown by Feenstra.[26]

Figure 3 shows NC curves for the as-deposited ITO film. Immediately evident is the absence of a zero conductance region, while there is a minimum at V_{bias}=+0.06 V, which implies the presence of slight band bending at the surface, since in the absence of band bending the minimum should appear at V_{bias}=0 V, corresponding to the Fermi level position E_F.

Moreover, the band gap edges (E_C and E_V) are resolved in the spectrum at +1.3 V and −1 V, respectively. This provides a value of the band gap around 2.3 eV, which is quite different from the direct bulk optical gap value of 3.7 eV well known from the literature,[25] and to the value of 3.56 eV found for thin films.[27] The value of 2.3 eV from our results is closer to the indirect band gap value (2.8–3.4 eV) and more consistent with the orange emission of ITO (bulk and film) at 1.9 eV.[20,21]

For bias voltage values lower than −1 V in the spectrum, we observe a shoulder located at −2.2 V (marked by the upward pointing arrow in Fig. 3) that could be related to the valence band edge of ITO, suggesting its direct electronic band gap value could be set at 3.5 eV.

Beyond the components of the conductance due to the tunneling through filled and empty states, we observe two different shoulders in the region of the gap. Similar features have been seen by Feenstra[26] for the clean surfaces of several III-V semiconductors. This nonzero conductance within the gap, the so-called *dopant-induced* component, has been ascribed to electrons tunneling through electronic states located near the band edge, whose contribution to the conductance is seen throughout the band gap because of the voltage dependence of the tunneling transmission term.

In our case, we found an electronic behavior remarkably different from that previously described for ITO,[28] and generally expected, from a heavily doped *n*-type semiconductor, with the Fermi level energy located close to the center of the gap. We suggest that Sn-doping impurities introduced in the In_2O_3 lattice and the oxygen vacancies derived from the reactive evaporation method, which determine the ITO electronic properties, can create a high density of defects, which induce localized electronic levels in the band gap. These midgap electronic states can shift the surface Fermi level towards the middle of the gap, pinning it at the energy level of the defect.

In the conduction band side of the STS spectrum, small peaks are observed at 2.1 V and 2.8 V (peaks *A* and *B* in Fig. 3); these sharp features could be related to cation-derived electronic states with significant surface character, essentially surface resonances, since they lie within the bulk conduction band.

For ITO annealed at 423 K, whose STS spectrum is shown in Fig. 4(a), the zero conductance region is still absent and the NC shows a minimum at V_{bias}=+0.03 V, suggesting a decrease of surface band bending with respect to the as-deposited sample.

Band gap edges (E_C and E_V) are resolved in the spectrum at +1.1 V and −0.8 V, and in addition in the valence band side of the spectrum we observe the same structures seen in Fig. 3, with a further shoulder at +1.5 V and an onset located

at +1.9 V in the conduction band side. We suggest that these additional structures are related to the ITO direct band gap. The band gap value is 1.9 eV, close to the band gap found for the as-deposited sample, but also for this sample we find the Fermi level position pinned close to the center of the gap and, additionally, we observe the dopant-induced component less clearly compared to Fig. 3. We assume that the annealing procedure induces changes, not only morphologically, as shown in Fig. 1(b), but also in electronic structure. In fact this dopant-induced component in the conductance spectra is a very sensitive measure of the surface quality, since a small shift of Fermi level position, due to any changes on the surface, can cause this component to disappear.[29]

Hence, the annealing procedure seems to cause a partial redistribution of the electronic states, as we can see from Fig. 4(a) where several peaks are present on both the conduction and valence band sides of the spectrum, with a residual disorder which could be responsible for the smaller shift of Fermi level position and the unpinning of the Fermi level from the middle of the gap.

The NC curve for ITO sample annealed at 573 K is shown in Fig. 4(b). The dopant-induced component in the conductance spectra has completely disappeared, leaving the typical zero conductance region of semiconducting materials. Band gap edges (E_C and E_V) are resolved in the spectrum at +1 V and –1.1 V, determining the band gap value as 2.1 eV, but once again the Fermi level remains pinned close to the center of the band gap. Small peaks are found in the spectra, located at different energy position [peaks $C-F$ in Figs. 4(a) and 4(b)] with respect to resonances A and B in Fig. 3. Given that peaks A and B are no longer apparent in the spectra in Figs. 4(a) and 4(b) and the presence of new features, it appears that the annealing processes cause a change in the surface electronic structure.

Previous studies on semiconductor interfaces[30] showed that annealing procedures enhance surface quality, reducing the band bending and the pinning position of Fermi level. For our ITO samples, we observed that the annealing procedure induces a substantial surface rearrangement, causing the dopant-induced component to disappear, but leaving unchanged the band gap value, in the range 1.9–2.3 eV, and the Fermi level pinned close to the midgap. This could suggest that the employed annealing temperature is not high enough to completely remove the defects inducing localized electronic levels in the band gap, and thus unpin the Fermi level position.

Optical measurements were carried out with the aim to find evidence for the indirect or direct nature of the electronic band gap of our ITO samples.[31] Figure 5 shows the measured transmission $T(h\nu)$ and specular reflection $R(h\nu)$ spectra acquired on an as-deposited ITO grown on Corning glass in the energy range 0.4 to 6.2 eV. We found $T(h\nu) \geqslant 80\%$ in a wide spectral range, 1.4–3 eV. $T(h\nu)$ drops off steeply for $h\nu \leqslant 1.4$ eV and $h\nu \geqslant 3$ eV. $R(h\nu)$ shows large oscillations, probably due to multiple reflections, in the photon energy range 1.4–5 eV.

The absorption coefficient $\alpha(h\nu)$ was calculated from $R(h\nu)$ and $T(h\nu)$ from the relationship

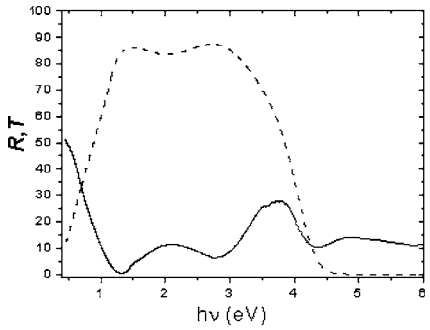

FIG. 5. Transmission $T(h\nu)$ (dashed line) and specular reflection $R(h\nu)$ (solid line) spectra of as-deposited ITO film grown on Corning glass.

$$\alpha(h\nu) = \frac{1}{l} \ln \frac{1 - R(h\nu)}{T(h\nu)}, \tag{1}$$

where l is the thickness of the film. Figure 6 shows $\alpha(h\nu)$ obtained from (1) in the energy range 0.4–4.5 eV. As $h\nu$ increases, α decreases down to about 1.7×10^3 cm^{-1} at 2.4 eV, increases slowly until the photon energy reaches about 3.5 eV, and then increases quickly to values above 10^5 cm^{-1}. The absorption in the low photon energy range ($h\nu < 0.5$ eV) has been found to be mainly due to intraband transitions, i.e., to free electrons in the conduction band.[31]

It is well known that for doping levels exceeding the charge carrier density set by the Mott criterion ($n \geqslant n_c \approx 10^{18}$ cm^{-3} for indium tin oxide), ITO can be considered as a semiconductor having a full valence band, with a parabolic conduction band partially filled by a degenerate free electron gas.[32]

Describing our system by a Drude free-electron model, the real and the imaginary parts of dielectric function $\varepsilon = \varepsilon_1 + i\varepsilon_2$ are given by[33]

$$\varepsilon_1 = \varepsilon_\infty - \frac{\omega_N^2 \tau^2}{1 + \omega^2 \tau^2}, \quad \varepsilon_2 = \frac{1}{\omega} \frac{\omega_N^2 \tau}{1 + \omega^2 \tau^2}, \tag{2}$$

where $\omega_N^2 = ne^2/\varepsilon_0 m^*, m^*$ is the free-electron effective mass, τ is the electron scattering time, n is the charge carrier density, and ε_0 and ε_∞ are the permittivity of free space and the high frequency relative permittivity of ITO lattice, respectively. We assume τ is approximately constant in the spectral

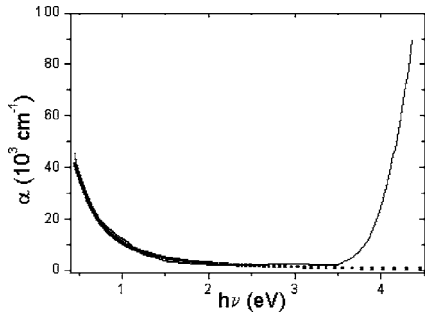

FIG. 6. Calculated absorption coefficient as function of photon energy for the sample of Fig. 5; the dotted line is the fitted Drude model curve.

range of our measurements, and electron scattering in the ITO film is essentially due to doping impurity ions acting as scattering centres.

We fit the experimental data for $h\nu \leqslant 2.5$ eV using the absorption coefficient α obtained from Eq. (2). The best fit gives for ε_∞, ω_N, and τ values of 4, 1.57×10^{15} s^{-1}, and 1.61×10^{-15} s, respectively, which can be used to determine the charge carrier density and the plasma frequency using the expression

$$\omega_N^2 = ne^2/\varepsilon_0 m^*, \quad \omega_p \approx \omega_N/\sqrt{\varepsilon_\infty}. \tag{3}$$

Using an effective mass $m^* \approx 0.35 m_e$,[32] we found a charge carrier density $n=2.7\times10^{20}$ cm^{-3}, as we expected for indium tin oxide,[34] and a plasma frequency $\omega_p=0.8\times10^{15}$ s^{-1}. Because of the high value of n, we can consider the ITO samples as highly degenerate semiconductors with the electron mobility due only to the contribution of ionized impurity scattering. The electron mobility and resistivity were found to be $\mu_e=23$ cm^2/V s and $\rho=9.8\times10^{-4}$ Ω cm.

As we have already mentioned, absorption in the low photon energy range should be mainly due to intraband transitions, which can be dealt with using the Drude model. We subtracted the Drude absorption α_D (gray line in Fig. 6) from the measured absorption α (black line in Fig. 6) to obtain information about interband transitions and the possible indirect band gap. The difference between α and α_D is in fact related to absorption due to interband transitions. We plot the square root of the difference $\alpha-\alpha_D$, which is expected to be linearly dependent on the photon energy for an indirect transition, vs photon energy in Fig. 7. $\sqrt{(\alpha-\alpha_D)}$ shows a linear trend at high photon energy with an onset around 3.4 eV and a further trend with photon energies decreasing from 2.8 eV indicating an indirect transition. Extrapolation to zero intensity gives a value of about 2.4 eV.

To understand if the onset at high photon energy corresponds to the direct band gap we plotted $(\alpha h\nu)^2$ vs $h\nu$ (inset Fig. 7). This quantity shows a linear trend with a threshold around 3.6 eV, indicative of a direct transition.[35,36]

The obtained threshold value for the direct and indirect transitions (3.6 eV and 2.4 eV, respectively) are consistent with the band gap values obtained from STS measurements.

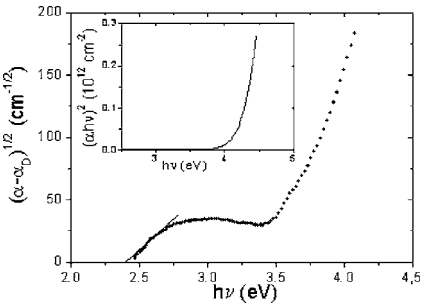

FIG. 7. Square root of $(\alpha-\alpha_D)$ as function of photon energy and corresponding $(\alpha h\nu)^2$ vs $h\nu$ for the sample of Fig. 5.

IV. CONCLUSIONS

In this work, we have performed a combined STM-optical study on indium tin oxide thin films deposited on silicon substrates by reactive electron-beam deposition. ITO films were studied by STM in ultrahigh vacuum after an annealing *in situ* at different temperatures in order to investigate the deviations induced on surface morphological and electronic structure by such procedure. Room temperature STM images on the as-deposited film show the surface composed of small grains with sizes of 30 nm, while STM images of annealed samples at 423 K and 573 K indicate that these grains coalesce into clusters with sizes of 60–80 nm upon increasing temperature, while the surface roughness values are in the range between 5–7 nm. STS analysis on the different areas of the surface suggests that the contrasts in STM images are mainly due to the sample morphologies. Furthermore, the normalized conductance spectra show a change in ITO LDOS of the annealed sample compared to the as-deposited ones. Significant variations in the dopant-induced component and zero conductance region can be observed, nevertheless the electronic band gap does not change. We suggest that the annealing procedure modifies the surface LDOS of ITO, but the process temperature is not high enough to unpin the Fermi level. Finally, optical absorption data obtained from reflectance and transmittance measurements has indicated an indirect transition around 2.4 eV. The combination of this result with STS measurements indicates an indirect band gap at 2.4 eV and a direct band gap at 3.6 eV.

*Corresponding author. Email address: francesca.matino@unile.it

[1] R. G. Gordon, MRS Bull. **25**, 52 (2000).
[2] J. S. Kim, M. Granström, R. H. Friend, N. Johansson, W. R. Salaneck, R. Daik, W. J. Feast, and F. Cacialli, J. Appl. Phys. **84**, 6859 (1998).
[3] M. Chen, Z. L. Pei, X. Wang, Y. H. Yu, X. H. Liu, C. Sun, and L. S. Wen, J. Phys. D **33**, 2538 (2000).
[4] C. G. Granqvist and A. Hultåker, Thin Solid Films **411**, 1 (2002).
[5] T. Ninami, MRS Bull. **25**, (8) 38 (2000).
[6] H. C. Lee and O. O. Park, Vacuum **75**, 275 (2004).
[7] N. Mori, S. Ooki, N. Masubuchi, A. Tanaka, M. Kogoma, and T. Ito, Thin Solid Films **411**, 6 (2002).
[8] J. S. Kim, F. Cacialli, M. Granström, R. H. Friend, N. Johansson, W. R. Salaneck, R. Daik, and W. J. Feast, Synth. Met. **101**, 111 (1999).
[9] T. Gerfin and M. Grätzel, J. Appl. Phys. **79**, 1722 (1996).
[10] T. Ishida, H. Kobayashi, and Y. Nakato, J. Appl. Phys. **73**, 4344 (1993).
[11] R. I. R. Blyth, F. P. Netzer, and M. G. Ramsey, Surf. Sci. **465**, 120 (2000).
[12] R. I. R. Blyth, F. P. Netzer, R. Resel, and M. G. Ramsey, Surf. Sci. **446**, 137 (2000).
[13] Y. Shigesato, S. Takaki, and T. Haranoh, J. Appl. Phys. **71**, 3356 (1992).

[14] S. Brewer and S. Franzen, J. Alloys Compd. **338**, 73 (2002).
[15] I. Hamberg, C. G. Granqvist, K. F. Berggren, B. E. Sernelius, and L. Engström, Phys. Rev. B **30**, 3240 (1984).
[16] O. N. Mryasov and A. J. Freeman, Phys. Rev. B **64**, 233111 (2001).
[17] L. A. Errico, M. Renteria, G. Fabricius, and G. N. Darriba, Hyperfine Interact. (to be published).
[18] M. Marezio, Acta Crystallogr. **20**, 723 (1966).
[19] S. Ray, R. Banerjee, N. Basu, A. K. Batabyal, and A. K. Barna, J. Appl. Phys. **54**, 3497 (1983).
[20] A. El Hichou, A. Kachouane, J. L. Bubendorff, M. Addou, J. Ebothe, M. Troyon, and A. Bougrine, Thin Solid Films **458**, 263 (2004).
[21] M. S. Lee, W. C. Choi, E. K. Kim, C. K. Kim, and S. K. Min, Thin Solid Films **279**, 1 (1996).
[22] J. Kane and H. P. Schweizer, Thin Solid Films **29**, 155 (1975).
[23] J. Lukkari, M. Alanko, L. Heikkila, R. Laiho, and J. Kankare, Chem. Mater. **5**, 289 (1993).
[24] D. Poelman and P. F. Smet, J. Phys. D **36**, 1850 (2003).
[25] S. Kasiviswanathan, V. Srinivas, A. K. Kar, B. K. Mathur, and K. L. Chopra, Solid State Commun. **101**, 831 (1997).
[26] R. M. Feenstra, Phys. Rev. B **50**, 4561 (1994).
[27] M. Penza, S. Cozzi, M. A. Tagliente, L. Mirenghi, C. Martucci, and A. Quirini, Thin Solid Films **349**, 71 (1999).
[28] S. Kasiviswanathan, V. Srinivas, A. K. Kar, B. K. Mathur, and K. L. Chopra, Appl. Surf. Sci. **115**, 399 (1997).
[29] J. A. Stroscio and R. M. Feenstra, J. Vac. Sci. Technol. B **6**, 1472 (1988).
[30] F. Schäffler, R. Ludeke, A. Taleb-Ibrahimi, G. Hughes, and D. Rieger, Phys. Rev. B **36**, R1328 (1987).
[31] H. A. Al-Brithen, A. R. Smith, and D. Gall, Phys. Rev. B **70**, 045303 (2004).
[32] I. Hamberg and C. G. Granqvist, J. Appl. Phys. **60**, R123 (1986).
[33] A. Porch, D. Vernon Morgan, R. Perks, M. O. Jones, and P. P. Edwards, J. Appl. Phys. **95**, 4734 (2004).
[34] R. B. H. Tahar, T. Ban, Y. Ohya, and Y. Takahashi, J. Appl. Phys. **83**, 2631 (1998).
[35] A. R. Smith, H. A. H. Al-brithen, D. C. Ingram, and D. Gall, J. Appl. Phys. **90**, 1809 (2001).
[36] D. Gall, I. Petrov, L. D. Madsen, J.-E. Sundgren, and J. E. Greene, J. Vac. Sci. Technol. A **16**, 2411 (1998).